Analyst

ROYAL SOCIETY OF CHEMISTRY

PAPER

View Article Online
View Journal

Cite this: DOI: 10.1039/d0an01545h

Probing amyloid fibril secondary structures by infrared nanospectroscopy: experimental and theoretical considerations†

Jehan Waeytens, *[a,b] Jérémie Mathurin, [b] Ariane Deniset-Besseau,[b] Véronique Arluison, [c,d] Luc Bousset,[e] Human Rezaei,[f] Vincent Raussens [a] and Alexandre Dazzi[b]

Received 3rd August 2020,
Accepted 4th October 2020

DOI: 10.1039/d0an01545h

rsc.li/analyst

Amyloid fibrils are composed of aggregated peptides or proteins in a fibrillary structure with a higher β-sheet content than their native structure. Attenuated total reflection Fourier transform infrared spectroscopy only provides bulk analysis of a sample therefore it is impossible to discriminate between different aggregated structures. To overcome this limitation, near-field techniques like AFM-IR have emerged in the last twenty years to allow infrared nanospectroscopy. This technique obtains IR spectra with a spatial resolution of ten nanometres, the size of isolated fibrils. Here, we present essential practical considerations to avoid misinterpretations and artefacts during these analyses. Effects of polarization of the incident IR laser, illumination configuration and coating of the AFM probes are discussed, including the advantages and drawbacks of their use. This approach will improve interpretation of AFM-IR spectra especially for the determination of secondary structures of species not accessible using classical ATR-FTIR.

1. Introduction

Amyloidosis is a group of pathologies induced by the aggregation of functional proteins. This aggregation is caused by a change in the conformation of proteins which leads to their misfolding. To date, more than 30 proteins are known to form aggregates that are responsible for various diseases such as Creutzfeld-Jacob, Alzheimer, Parkinson, type II diabetes or some cancers.[1] Amyloids are rich in cross-β sheet structures, with percentages that depend on the protein, and they assemble to form insoluble fibrils.[2] Amyloid fibrils can have different lengths but their width is invariant between 8 to 10 nm. Structural analysis of amyloid nano-assemblies is essential for understanding their behavior and pathogenicity. For example, dimers, trimers, and tetramers of amyloid β proteins (Aβ) are called oligomers and higher size aggregates with a bead-like form up to 200 nm in length are called protofibrils, which are toxic to neurons and their vital interconnections[3,4] whereas longer fibrils can induce an inflammatory response, a process that actively contributes to the toxicity of amyloidogenic proteins.[5–7] Unfortunately, fibrils are difficult to study with the most commonly used high-resolution structural methods (X-ray diffraction, solid-state nuclear magnetic resonance and cryo-electronic microscopy) as these methods are not suitable for insoluble material or species in equilibrium between different types of aggregates. Vibrational spectroscopy, more specifically infrared (IR) spectroscopy, provides interesting alternatives. IR probes molecular vibrations and for decades has been extensively used to study protein secondary structures,[8] including aggregates.[9]

The IR response of proteins and analysis of their secondary structure are well-known.[10] Usually, spectral shape differences in the amide I and amide II regions are investigated. In the case of the amide I region, all different secondary structures absorb in a specific range due to different transition

[a]Structure et Fonction des Membranes Biologiques, Université libre de Bruxelles, Bruxelles, Belgique. E-mail: jehan.waeytens@ulb.ac.be
[b]Institut de Chimie Physique d'Orsay, CNRS UMR8000, Université Paris-Sud, Université Paris-Saclay, Orsay, France
[c]Laboratoire Léon Brillouin LLB, CEA, CNRS UMR12, Université Paris Saclay, CEA Saclay, 91191 Gif-sur-Yvette, France
[d]Université de Paris, 75006 Paris, France
[e]Paris-Saclay Institute of Neuroscience, CNRS, Avenue de la Terrasse, 91198 Gif-sur-Yvette, France
[f]Institut National de la Recherche Agronomique (INRA), Unité de Virologie et Immunologie Moléculaire, Jouy-en-Josas Cedex, France

†Electronic supplementary information (ESI) available: Figures including the AFM images of the different amyloid fibrils studied, the AFM-IR spectra without normalization to observe the gold enhancement, all the fitting of the different spectra for secondary structures and the Hfq spectra with the different AFM-IR setup and tips. See DOI: 10.1039/d0an01545h

Table 1 Assignment of amide I band based on experimental data from various research teams and extracted from the review of Goormaghtigh *et al.*[12]

	Band position in H_2O (cm^{-1})	
Secondary structure	Center	Range
α-Helix	1654	1648–1657
β-Sheet	1633	1623–1641
	1684	1674–1695
Turns	1672	1662–1686
Disordered	1654	1642–1657

dipole coupling with the peptide backbone, as specified in Table 1.[11]

In order to differentiate the different types of aggregates that compose a fibrillar sample, IR microscopy should be used. However, it can only achieve micrometric lateral resolution at best, which is far below the size of the aggregates. Within the last twenty years, several super-resolution near-field techniques,[13] derived from atomic force microscopy, have emerged overcoming these limits of classical vibrational microscopies as well as allowing analysis of highly heterogeneous systems. Among these different technologies, AFM-IR (atomic force microscopy based IR spectroscopy),[14] that detects a photothermal effect, seems to be the most relevant and robust to study amyloid fibrils.[15–20] Indeed sSNOM (scattering near-field optical microscopy) technology is more comparable to GI-FTIR (grazing angle incident FTIR) analysis where polarization effects are dominant. In GI-FTIR and sSNOM, mainly the vibrations oriented along the vertical axis of the surface is probed.[14]

In the past 10 years, AFM-IR has continuously evolved and improved. Nowadays, two configurations coexist: the first is characterized by a configuration with a bottom-up illumination,[21] and the second utilizes a top-down illumination.[22] Simultaneously, the evolution of IR laser sources opened new possibilities and the resonance enhanced mode was developed, offering tremendous improvement in terms of sensitivity and resolution.[22] The AFM probe used by different AFM-IR configurations could also play a role in the measurement. Indeed, for the first configuration (bottom-up) silicon-tips are used whereas gold-coated tips are preferred for the system using top-down illumination.

But those advances are not without consequences. In recent papers using AFM-IR,[16–20] analysis on amyloid fibrils with those different setups provided different spectra and interpretation. For example, results obtained by Henry *et al.*[18] or Ruggeri *et al.*[16] differ. Ruggeri *et al.* published a work on the Josephin domain of Ataxin-3 using a bottom-up illumination and a silicon-probe.[16] During the aggregation of this protein, they observed an increase of the 1690–1710 cm^{-1} region assigned to the anti-parallel β-sheet structure. A second publication from Ruggeri *et al.* deals with polyQ tracts in the first exon of the huntingtin protein. The study was performed using a top-down illumination and a decrease of the absorption band in the 1663–1659 cm^{-1} range was observed as well as an increase of two bands at 1692 and 1684 cm^{-1}, respectively assigned to an antiparallel β-sheet and β-turns.[17] Henry *et al.* performed experiments using bottom-up illumination and a gold-coated tip and studied the Aβ42 peptide and its interaction with lipids.[18] They studied fibrils formed from wild-type Aβ and a mutant in oligomer conformation. For the wild type, they observed a major band at 1631 cm^{-1} associated with β-sheet aggregated structures and another one at 1662 assigned to β-turns. For the mutant, a shoulder at 1689 cm^{-1} mixed with β-turns at 1662 cm^{-1} appeared. The effect of the substrate used in AFM-IR was discussed previously.[20] The nature of some surfaces like ZnSe used in bottom-up illumination induces amyloid sample destructuring, leading to amorphous aggregates. The substrate nature should be carefully selected to study amyloid fibrils. The ZnS prism should be preferred for AFM-IR or a gold surface with top-down illumination. With these two substrates, the different amyloid fibrils have a similar shape and length as on standard mica surfaces. More recently, Partouche *et al.* studied the C-terminal region of a bacterial (*Escherichia coli*) protein Hfq that forms functional amyloid like fibrils, with a top-down illumination.[19] They were able to follow the β-sheet content using the ratio between the β-sheet structure absorption band at 1620 cm^{-1} and the maximum of the amide I band at 1660 cm^{-1}.

It is clear there are differences in spectra and interpretation for these studies of different β-sheet structures. Those different results and spectral signatures have never been deeply discussed or explained. For the consistency of the technique, it seems important to determine what are the factors that influence or disturb the infrared spectra obtained by AFM-IR. If we compare all these results, parameters which change from one study to another are: (i) the AFM-IR configuration, (ii) the tip properties and (iii) the β-sheet content of the fibrils. To understand the role and influence of the different parameters, we present a study that compares fibril spectra obtained by different AFM-IR configurations and setup. A discussion is presented about the consequences of their secondary structure analysis. For this purpose, 3 different amyloid fibrils were studied: (i) amyloid β 1–42 peptide (Aβ),[23,24] (ii) α-synuclein (α-syn),[25–27] and (iii) the ovine prion (PrP).[28–31]

We first describe the different AFM-IR configurations, then illustrate the effect of the laser polarization state on the local IR response of the fibrils. The effect of a gold-coated AFM probe is discussed by modelling and comparing the spectra obtained on the 3 different fibrils. Finally, we compare the structural analysis obtained using ATR-FTIR spectra with the one obtained using AFM-IR data: first for Aβ, α-syn and PrP and then for a functional amyloid-like nano-assembly formed by the C-terminal part of the bacterial protein Hfq.

2. Methods

2.1 Aβ sample preparation

WT Amyloid β 1–42 was purchased from Bachem (Bubendorf BL, Switzerland). Aβ peptides were dissolved in cold hexa-

fluoroisopropanol (HFIP) at a concentration of 2 mg mL^{-1} and incubated for 1 hour at room temperature. HFIP was removed first under nitrogen flow and then using a Speed Vac (Fisher Thermo Savant, Waltham, MA, US) for 1 hour. Peptides were dissolved in dimethylsulfoxide at a final concentration of 5 mM and then diluted to a final concentration of 100 μM in HCl 10 mM. Peptides were incubated at 37 °C for 1 week.[58] The solution was diluted by a factor of 1000 in mQ water. Fibrils were deposited on a ZnS prism or gold substrate and dried at room temperature under light airflow.

2.2 α-Synuclein sample preparation

Recombinant wild-type α-syn was expressed in *E. coli* BL21 (DE3) strain (Stratagene, La Jolla, CA, USA), transformed with the expression vector pET3a (Novagen, Merck, Darmstadt, Ge) encoding wild-type, full-length α-syn. The expression of α-syn was induced by 0.5 mM IPTG for 2 h, when the bacteria, grown in LB medium at 37 °C, reached an optical density of 1.0 at 660 nm. Soluble, monomeric α-syn was purified from the bacterial lysate as previously described.[59] α-Syn concentration was determined spectrophotometrically using an extinction coefficient of 5960 M^{-1} cm^{-1} at 280 nm. Pure α-syn (0.2–0.5 mM) in 50 mM Tris-HCl, pH 7.5, 150 mM KCl was filtered through sterile 0.22 μm filters and stored at −80 °C. α-Syn in different buffers, (see below) and was incubated for one week at 37 °C under continuous shaking in an Eppendorf Thermomixer set at 600 rpm to assemble into distinct fibrillar polymorphs. To obtain the polymorph "fibrils", α-syn (400 μM) was assembled in 50 mM Tris-HCl, pH 7.5, 150 mM KCl buffer. This solution was diluted by a factor of 1000 in mQ water. Fibrils were deposited on a ZnS prism or gold substrate and dried at room temperature under light airflow.

2.3 Prion sample preparation

PrP amyloid fibrils were formed using the manual setup protocol described previously.[60] Briefly, the lyophilized protein was dissolved directly in 50 mM MES buffer, pH 6.0 at 1 mg ml^{-1}. Tris solution was kept on ice before starting the experiment. To prepare a 500 μl reaction mixture, the following reagents were mixed in a conical plastic tube: water (90 μl), guanidine-HCl (6 M, 200 μl), MES buffer (0.5 M, pH 6.0, 10 μl) and finally the PrP stock solution (300 μl). The solution was mixed by gently pipetting to avoid introducing air bubbles. Typically for the PrP stock solution, a 10 ml reaction was made in a 15 ml conical centrifuge tube. The tube (arranged horizontally on the plate surface) was incubated with continuous orbital shaking at 30 rpm (16 mm amplitude) at 37 °C. Fibril formation was monitored using a Thioflavin-T (ThT) binding assay.[61] For this assay, aliquots were withdrawn and diluted in 10 mM Na-acetate buffer, pH 5.0 to a final concentration of PrP of 0.3 μM. Then ThT was added to a final concentration of 10 μM. Samples were dialyzed in 10 mM sodium acetate, pH 5.0. Then fibrils were collected by ultracentrifugation for 45 min at 228 147*g* using a Beckman Optima TL100 Ultracentrifuge and TLA-100.3 rotor (Beckman Coulter, Pasadena, CA, US), and resuspended in 10 mM sodium acetate, pH 5.0. A washing step was performed by repeating the ultracentrifugation and resuspension steps. All concentrations given for fibrillar PrP refer to the respective equivalent monomer concentration.

2.4 Hfq sample preparation

The fibrils of the peptide corresponding to the CTR domain of *E. coli* Hfq (residues 64–102, SRPVSHHSNNAGGGTSSNYHHGSSAQNTSAQQDSEETE) were purchased from Proteogenix (Schiltigheim, Fr).[45] Hfq peptide was reconstituted in water at 20 mg ml^{-1}. This solution was diluted by a factor 1000 in mQ water. Fibrils were deposited on a ZnS prism or gold substrate and dried at room temperature under light airflow.

2.5 Analysis by AFM-IR

Sample were analyzed using an AFM-IR system with two different illumination available (bottom up and top-down). For bottom-up illumination, the system used was a nanoIR1 from Anasys Instruments (Bruker, Billerica, MA, US). The sample was deposited on a ZnS prism (SM-nIR-Prism2 from Bruker), with illumination in attenuated total reflection. The laser used was a QCL from Daylight Solution (San Diego, CA, US) with one chip centered at 1650 cm^{-1}. 100% of the laser power was used with a co-averaging of 128 and a duty cycle around 20%. The AFM probe used for the experiment was purchased from μmasch (Tallinn, Estonia) with a spring constant around 0.03 N m^{-1} (reference HQ:CSC38/Al-BS and HQ:CSC38/Cr-Au for gold coated tips).

For the top-down illumination, the equipment used was a nanoIR2 from Anasys Instruments. The sample was deposited on a gold substrate (Platypus Technologies Au.1000.SWTSG, Fitchburg, WI, US). The laser used was a QCL mircat-QT from Daylight Solutions and a HQ:CSC38/Cr-Au gold coated tip was used.

All AFM-IR spectra presented are the average of 25 different spectra acquired on fibrils with all orientations in the *XY* plane (1 spectrum per fibril). The average spectra were smoothed with a double-Gaussian filter with a cut-off of 2.5 cm^{-1} with Mountains Map 8 (Digital Surf, Besançon, FR). To better show difference in the spectra, all the spectra were normalized on the area of the amide I band (from 1700 to 1600 cm^{-1}).

The spectrum shown in Fig. 2b is the average of 8 spectra on the Y-aligned fibril between the red arrows as shown inFig. 2a. The solid line is the spectra made smooth with a double-Gaussian filter with a cut-off of 2.5 cm^{-1} and the slightly transparent line is the raw data corrected for water vapor with a local de-glitch filter at 1635 and 1682 cm^{-1}.

2.6 Modeling using COMSOL

The COMSOL (Grenoble, Fr) model is based on quasi-static approximation. The electric field is modeled with the 3D AC/DC module. As the space of the study is smaller than 100 nm, the electromagnetic field is considered constant. Gold is defined by a specific dielectric constant (negative). Amyloid Fibrils have been modelled in a cylinder shape with a 10 nano-

meter diameter and with poly(methyl methacrylate) material parameter.

2.7 ATR-FTIR measurement

Attenuated total reflection Fourier transform infrared spectra were recorded on a Bruker Equinox 55 infrared spectrophotometer equipped with a MCT detector at a resolution of 2 cm^{-1}. The spectrometer was continuously purged with dry air. The sample was dried on a Specac (Orpington, UK) diamond with a flux of dry air and 128 scans were averaged for the sample and background. The results were treated with kinetics for baseline correction, area normalization on the amide I band curve fitting, and unsupervised hierarchical clustering based on the Euclidean distance between the spectra. The spectra were plotted with OriginPro 2016 software (Northampton, MA, US).

2.8 HCA and deconvolution of the infrared spectrum

The hierarchical cluster analysis and deconvolution were carried out using Kinetics, a custom-made program, developed in our laboratory by Prof. Erik Goormaghtigh (SFMB, Université libre de Bruxelles, Belgique) running under Matlab (Mathworks, Natick, Ma, US). The analysis was done on the amide I region from 1700 to 1600 cm^{-1} after baseline correction and scaling of the spectra. For the deconvolution 5 peaks were used, two bands were used corresponding to loop and turns with a position between 1682 and 1662.5 cm^{-1}, α-helix between 1662 and 1645 cm^{-1}, random structure between 1644.5 and 1637 cm^{-1}, and one for the β-sheet between 1637 and 1610 cm^{-1}. The function used for the fitting is a mix of a Lorentzian and Gaussian function, and the ratio of the two functions is optimized from pure Gaussian to pure Lorentzian and starts with a 50/50 mix. The percentage of each structure corresponds to the area of the band normalized to 100%.

3. Results and discussion

3.1 AFM-IR configurations

In order to clarify the different results reported in the literature regarding amyloid-like nano-assemblies, we performed our study using the two illumination setups commercially available. The first involves illumination from the bottom side of the probed sample (called bottom-up illumination) and the second illumination from the top side (called top-down illumination). The bottom-up illumination uses an infrared transparent prism (ZnSe, ZnS, CaF_2...) similar to the attenuated total reflection technique used in IR spectroscopy. Moreover, the sample thickness must be lower than 1 micrometer to keep the illumination constant over the sample.[32] In our study, this constraint is not a limitation considering the size of fibrils. Furthermore, with this setup, both regular AFM silicon tips (Si-tip) and gold-coated Si-tip (Au-tip) can be employed. The top-down illumination is more versatile. All substrates transparent or reflective in the IR range are compatible and the sample thickness has no limitation, but as the Si-tip may absorb the IR radiation, exclusively the Au-tip is used. Currently, the top-down illumination system is the most common.

Amyloid-like nano-assemblies are highly oriented. Thus, IR linear dichroism analysis of amyloid fibrils provides information on their orientation.[33] Their cross β-sheet structure, which absorbs around 1620 cm^{-1}, is perpendicular to the fibril's long axis; the carbonyl (C═O) of the peptide bond is in the axis of the fibril. In the bottom-up illumination system, the polarization of the laser can be controlled and set to p-polarization (into the incident plane called *XZ*) or s-polarization (into the *XY* plane) (see Fig. 1). Due to the prism geometry, the incidence angle of illumination is fixed at 45°. Thus, if the laser polarization is p, the electric field is divided in two components at the surface of the prism: one along the *Z*-axis (P_z) and another one along the *X*-axis (P_x). For the s-polarization, only one contribution exists along the *Y*-axis (P_y).

As a consequence, for highly oriented material such as fibrils, the incident light polarization will have an effect on the IR response. In the case of fibrils aligned along the *Y*-axis (represented by a red line (Fig. 1a and b) and between red arrows (Fig. 2a – called Y-aligned fibrils), carbonyl vibrations of the amide I band of the β-sheets will be oriented along the same axis as the electric field for the s-polarization and perpendicularly for the p-polarization.[34] Under these conditions, we expect that these fibrils will present an important absorption signal due to the β-sheet structure only with the s-polarization. Experimentally, this behavior was observed with α-syn fibrils (high β-sheet content). In Fig. 2, at s-polarization, the maximum of the amide I band of the IR spectra acquired on a Y-aligned fibril (red arrows Fig. 2a) was centered at 1627 cm^{-1} with shoulders at higher wavenumber corresponding to the rest of the protein structure. At p-polarization the signal to noise ratio is low, the amide I absorption band was centered at 1650 cm^{-1}, and it is difficult to distinguish the absorption band at 1630 cm^{-1} of the β-sheet structures. In the case of X-aligned fibrils, carbonyl vibrations of the amide I band of the β-sheet are oriented along the *X*-axis. Thus, we do not expect to detect any absorption of the structure with a s-polarization and a weak one with a p-polarization as only one third of the electric field is X-aligned. Experimentally, the signal to noise ratio was indeed so low, for both cases, that it was impossible to extract a significant spectrum with relevant structural information. For the other analyses presented with structural determination, spectral averaging was used with spectra recorded at many different locations on fibrils and a better signal to noise ratio was therefore obtained.

With the top-down illumination system, the polarization is fixed with a p-polarization with a 70° incident angle (to the normal of the surface). Thus, fibrils oriented along the *Y*-axis should not present any IR absorption and the X-aligned only showed a weak one as only one third of the incident energy will highlight them.

3.2 AFM-IR study: bottom-up illumination with an Si-tip

In this section, we explore the response of 3 fibrillar samples with the bottom-up illumination configuration:

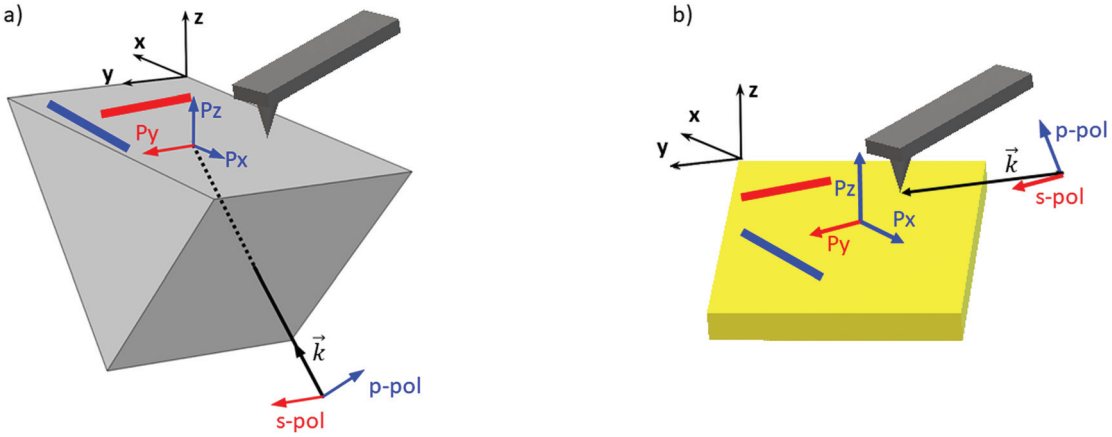

	Px	Py	Pz
p-pol	-1/3 P	0	2/3 P
s-pol	0	P	0

	Px	Py	Pz
p-pol	0.34 P	0	0.94 P
s-pol	0	P	0

Fig. 1 AFM-IR setups and orientation of polarization components: schematic view of the different AFM-IR illumination systems. (a) The bottom-up illumination, where IR laser comes from the bottom side (vector *k*) with the resulting electric field at the prism surface as a function of the incident laser polarization (blue for p-polarization, red for s-polarization). (b) The top-down illumination. On both, fibrils are represented in red when aligned along the *Y*-axis and in blue when oriented along the *X*-axis.

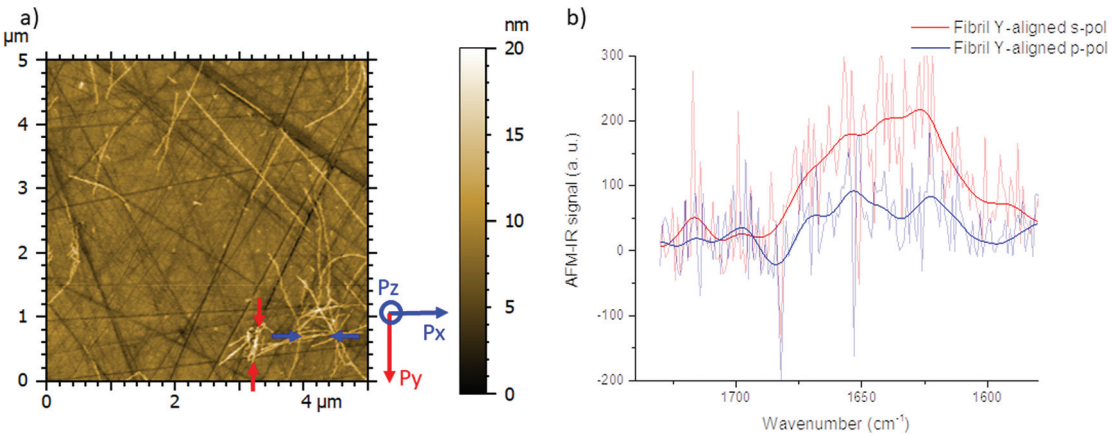

Fig. 2 Polarized-resolved AFM-IR study of α-syn fibrils with bottom-up illumination on the ZnS prism obtained at s- and p-polarization with the Si-tip. (a) Topography of the amyloid fibrils in contact mode with a HQ csc38 tip (0.03 N m^{-1}) at a constant load of 15 nN. Their orientations are indicated with blue and red arrows. (b) Averaged spectra of Y-aligned fibrils: acquisition all along the fibrils localized between the two red arrows at p- (blue spectrum) and s-polarization (red spectrum).

- Aβ is a 42 amino acid peptide involved in Alzheimer's disease and found in senile plaques with a high β-sheet content.[23,24]

- α-synuclein is a 140 amino acid protein and its aggregated form is found in Lewy bodies and neuritis, the pathological signature of Parkinson's disease.[25–27]

- PrP is a 240 amino acid protein involved in spongiform encephalopathies and characterized by a conformational change from α-helix to β-strand of the PrP^c to the endogenous scrapie form, which aggregates into amyloid plaques. Even if the protein is aggregated, the N-terminal region remains unstructured.[28–31]

IR spectra of Aβ, α-syn and Prp fibrils are shown in Fig. 3. They correspond to an average of 20 spectra normalized by the amide I band area. They were acquired on different fibrils in all orientation (on the prism) as it was impossible to observe pure X or Y-aligned fibrils.

For these three proteins, some discrepancies between p and s laser polarization are observed but the spectra present a common feature that the amide I band maximum is centered at around 1630 cm^{-1}. Usually, this maximum corresponding to the β-sheets is present between 1630 and 1610 cm^{-1}.[35] Spectral shifts observed for this band may be induced by a change in the secondary structure of the protein as well as difference in

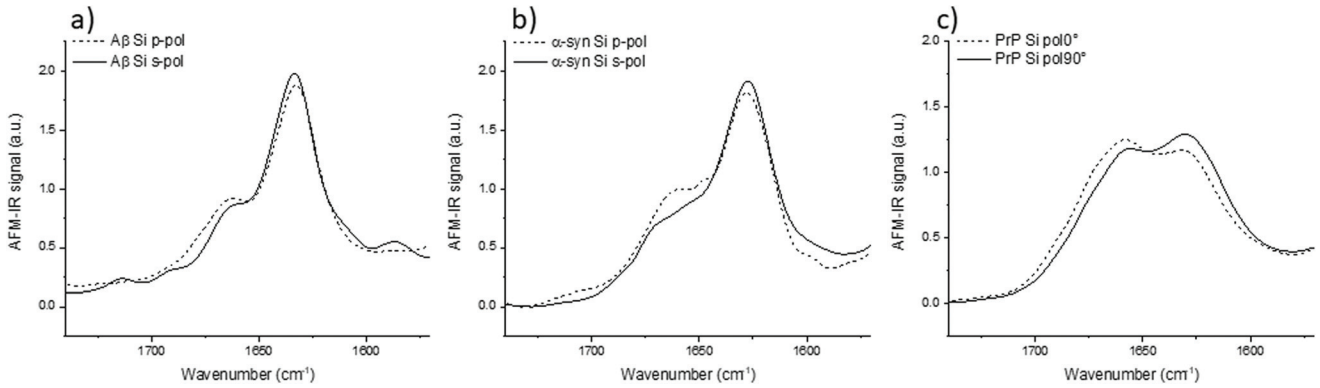

Fig. 3 AFM-IR analysis of amyloid fibrils obtained with bottom-up illumination, Si-tip on ZnS prism at s- and p-polarization. Normalized on amide I spectra of the 3 different proteins obtained with bottom-up illumination and Si-tip (a) Aβ, (b) α-syn and (c) PrP. Solid lines are for s- and dashed lines for p-polarization.

hydrogen bonding, and the number and length of β-strands involved in the β-sheet structure.

The amplitude differences are due to the percentage of amino acids involved in the β-sheet structure. Aβ has 58% of its amino acids involved in the β-sheet structure; α-syn, 75%; and PrP, 43%.[25,36,37] Upon more careful scrutiny of the spectra's shape obtained with a s-polarization, we observe that the Aβ amide I band is centered at 1632 cm^{-1} with a shoulder at 1662 cm^{-1} related to turns or unordered structures, which are in good agreement with ATR-FTIR measurements.[24] For α-syn, the amide I band is centered at 1627 cm^{-1}, again with a shoulder at 1662 cm^{-1}.[38,39] Whereas, PrP fibrils exhibit an amide I band centered at 1659 cm^{-1}, which indicates a major contribution of the unstructured part as well as remaining α-helix. The PrP spectrum also presents a maximum of absorption at around 1629 cm^{-1} corresponding to its β-sheet structure.[40]

With a p-polarization, the amplitude of the β-sheet band is 10% lower for all proteins compared with s-polarization. The difference is more pronounced for PrP fibrils where the β-sheet absorption band becomes less intense than the 1660 cm^{-1} band. Some of those differences, sometime at the same level as the noise, confirm a general trend that the objects present a relative orientation towards the electric field. Thus, the s-polarization seems to be the best configuration to study the β-sheet content of amyloid fibrils. The increase of amplitude for the β-sheet band can also be observed by polarized ATR-FTIR. The deposition of the amyloid fibrils is not controlled and bundles of fibrils are probably present, nevertheless the majority of fibrils lays on the ATR crystal. This preferred orientation allows seeing differences by using polarized ATR-FTIR. The β-sheet band is higher with p-polarization as shown in Fig. SI 2.†

3.3 Simulation of the local electric field nearby the fibrils

Currently, most infrared studies of objects below 100 nm size are performed with an AFM-IR system using a top-down illumination with an Au-tip as a probe.[15–17,41]

As reported in the literature, gold coating enhances the electric field at the apex of the tip by a factor up to two orders of magnitude with a p-polarized light.[42] Thus, a gain in signal is observed. The generally accepted idea is this gain helps to improve sensitivity and allows acquiring an IR image with a decent contrast, which is not possible with a Si-tip. However, impacts of gold coating, with or without polarized illumination, have not been fully investigated. For example, differences may occur using p-polarization compared with the s- one as the electric field is not towards the tip but perpendicular, this will affect the enhancement.

To understand the lightning rod effect of the Au-tip, a finite element simulation (COMSOL Multiphysics®) was performed. The goal is to model the distribution of the local electric field as a function of the polarization of the incident light. This model is valid for both AFM-IR configurations (bottom-up and top-down). As shown in Fig. 4, the simulated electric field under the Au-tip is 100-times more intense than the incident electric field and is spatially limited to a few nanometers around the tip apex. For a pure p-polarization (p-pol), gold coating induces a spreading of the electric field just below the apex and the direction of the field lines show a slight curvature (Fig. 4a and b). This curvature of the electric field adds an electric field component along the fibrils axis that might be absorbed by the carbonyl groups present in this direction. Therefore, it should be possible to amplify the β-sheet absorption band for an X-aligned fibril even with a p-polarization, due to both the enhancement and orientation of the resulting local electric field ($Ex \neq 0$). For a pure s-polarization (s-pol) with a Y-aligned fibril in the bottom-up configuration or P_x polarization in the case of the X-aligned fibril in top-down polarization, the behavior of the electric field is hyperbolic (Fig. 4c and d). It tends to zero under the apex of the tip. Thus, the illumination is no longer homogeneous, probing about only 2/3 of the fibrils. In this case, the signal detected mainly originates from the carbonyl bonds close to the support surface and not to the tip (Fig. 4d) making this type of analysis not easy to interpret. Additional simulations with gold sub-

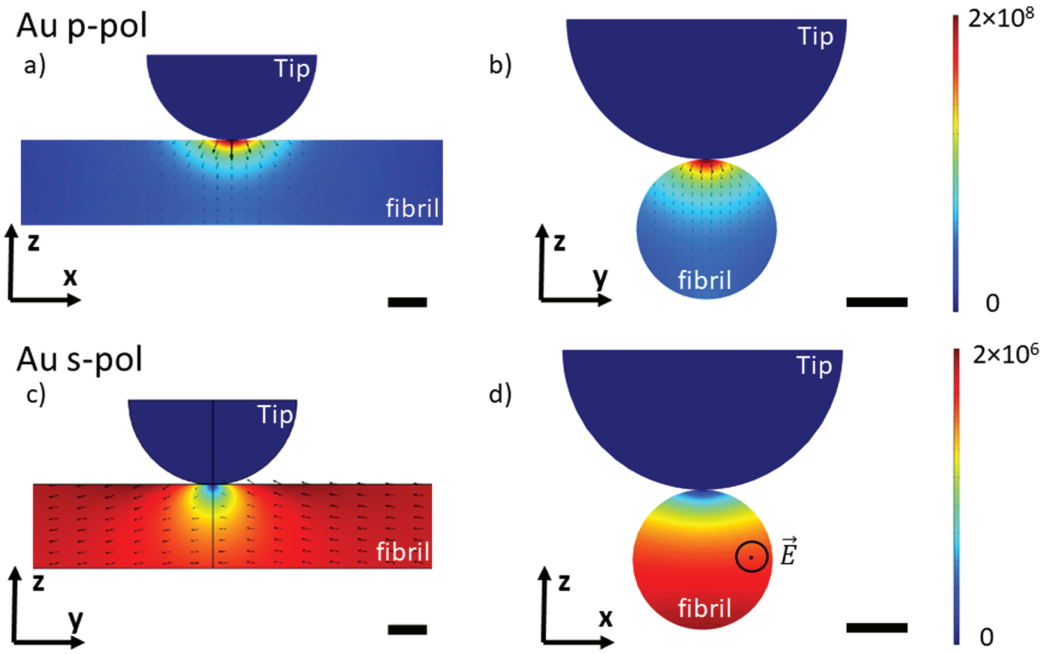

Fig. 4 Finite element simulation of the electric field induced in fibrils by an Au-tip: p-polarization (a) cross-section along the fibril axis (b) perpendicular cross-section; s-polarization (c) and (d). Electric field intensity (colored scale) and orientation (arrows) are represented only in the fibril. Scale bar 5 nm. (d) The electric field is perpendicular to the cross-section.

strate show that this sort of substrate does not change the direction of the electric field (Fig. SI 3†) and has only a minor effect on the intensity distribution in p-pol. This confirms that the gold tip prevails on the electric field distribution.

Those simulations show that the use of the Au-tip renders the illumination difficult to predict. Indeed, the real electric field enhancement is also related to the tip shape (here defined as a perfect sphere) which is never known and cannot be predicted or quantified. The estimation of the real orientation and amplitude of the local electric field is complex. Under this condition, it will clearly lead to misinterpretation of spectra of nanometric-size and highly oriented samples obtained with a system using an Au-tip.

3.4 AFM-IR study: bottom-up illumination with an Au-tip

Models have highlighted the complex orientation of the electric field when using an Au-tip. It generates a heterogeneous enhancement through the fibril. To illustrate these complex effects, AFM-IR spectra of amyloid fibrils are shown in Fig. 5, which compares the results obtained with the system using a bottom-up illumination either with an Si-tip or an Au-tip. We observe an absorption signal around 2× larger with the Au-tip than with the Si-tip. AFM-IR spectra were normalized by the area of the amide I band (Fig. SI 2†).

With both tips and polarization, the Aβ fibrils exhibit spectra with a high absorption centered at 1632 cm^{-1} with a shoulder at around 1662 cm^{-1}. Nevertheless, with the Au-tip,

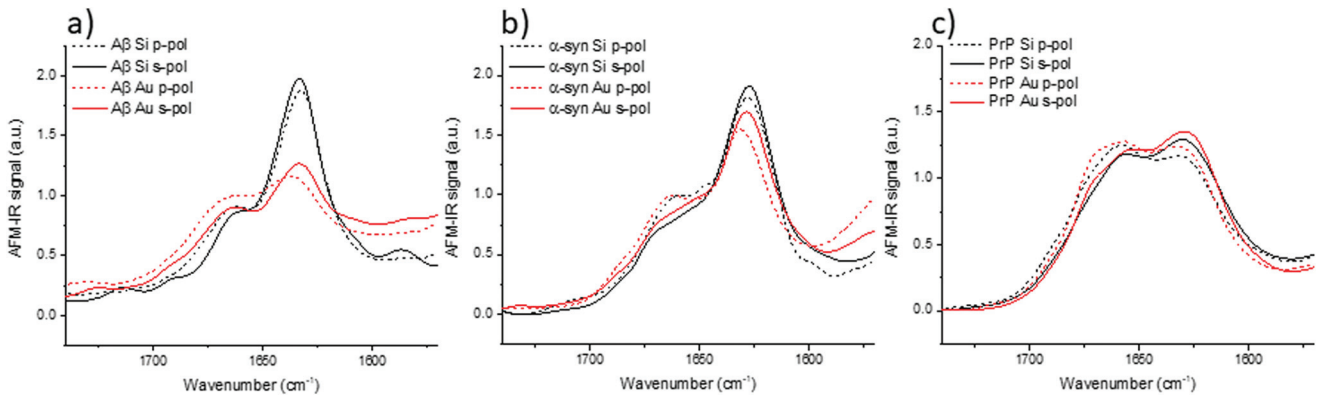

Fig. 5 Au-tip enhancement: normalized AFM-IR spectra of amyloid fibrils of (a) Aβ, (b) α-syn; (c) PrP. Black curve corresponds to Si-tip, red curve to Au-tip – solid lines for s-pol and dashed lines for p-pol. All results were obtained with bottom-up illumination.

the ratio between the 1632 cm^{-1} band and the 1662 cm^{-1} band ($A_{1632/1662}$) differs from the one measured using a Si-tip: $A_{1632/1662}$ for Si-tip are 2.3 and 2.1 and for Au-tip are 1.4 and 1.2 for s-pol and p-pol, respectively. α-Syn fibrils also have two major bands centered at 1627 cm^{-1} and 1662 cm^{-1}. The behavior due to changes in polarization is the same as that of Aβ, but the differences in terms of intensity are smaller between the Si-tip and Au-tip. The $A_{1627/1662}$ ratio is 2.0 with the Au-tip compared with 2.5 obtained during Si-tip measurements. For PrP fibrils, we observe the two bands centered at 1629 and 1659 cm^{-1} with both polarizations and tips but the 1629 cm^{-1} band is slightly higher with s-pol. The effect of Au-tip on PrP protein is not significant as, the $A_{1627/1662}$ ratios for the Au and Si-tip are close to 1.1 with s-pol and 0.9 for p-pol.

The effects of using an Au-tip on spectra seem to be difficult to interpret; with an Au-tip, the $A_{1627/1662}$ for α-syn and Aβ are damped whereas PrP fibrils seem to be unaffected. Either the proportion of β-sheet is lower in PrP protein or the secondary structure fibrils are more heterogeneously distributed along his diameter, which can lead to changes in the spectra due to the local enhancement observed with the simulations (Fig. 4c). Consequently, the use of an Au-tip in bottom-up illumination globally disturbs the intensities of some absorption bands (especially β-sheet) and should be employed with extreme caution if not prohibited when a fitting procedure is employed for secondary structure determination. The use of this setup is possible for qualitative study (benefit from the Au enhancement), but the results obtained cannot be extrapolated from one protein to another as the evolution of the band ratio is highly dependent of the inner structure of fibrils (as seen in Fig. 5).

3.5 AFM-IR study: bottom-up *versus* top-down illumination

The top-down illumination is preferred by users as it is more versatile and seems to offer a better signal to noise ratio. Thus, to study nano-assemblies, this configuration seems to be more appealing.

The results obtained with the top-down illumination (Fig. 6) highlight huge discrepancies between both configurations. With top-down illumination for Aβ and α-syn, the amide I band is centered at 1655 with a shoulder at 1680 cm^{-1} and a smaller one at 1632 cm^{-1}. Whereas with the bottom-up illumination, amide I is centered at 1632 cm^{-1} with a shoulder at 1662 cm^{-1}. For PrP, those discrepancies are weaker: the amide I band is centered at 1652 cm^{-1} with two shoulders at 1640 cm^{-1} and 1680 cm^{-1}, whereas it is clearly composed of two maxima centered at 1659 and 1620 cm^{-1} with the bottom-up illumination configuration.

For the three species, the shape of the amide I band obtained with the top-down illumination is not comparable to the one obtained with bottom-up illumination. The β-sheet absorption band (1630–1610 cm^{-1}) is either drastically lowered and/or shifted to a higher frequency or even absent in all spectra obtained with top-down illumination (blue curves in Fig. 6). The more pronounced differences can be observed for α-syn and Aβ. The maximum of the spectra is shifted from 1630 cm^{-1} to 1655 cm^{-1}. Noteworthy, a technical artefact is also present in those spectra. A shoulder around 1680 cm^{-1} arises due to the transition between two stages of the QCL laser source belonging to the top-down illumination equipment (different for bottom-up illumination system).

With this configuration, we can observe also a new weak shoulder on Aβ and α-syn spectra around 1720 cm^{-1}. It has been previously reported by Ruggeri *et al.* at around 1710 cm^{-1} for huntingtin.[17] Partouche *et al.* have also reported a peak at 1745 cm^{-1} and proposed it was assigned to a synthesis contamination (trifluoroacetic acid).[19]

We notice that this specific band is revealed with the system using a top-down illumination in our experiments but was observed in top-down and bottom-up illumination by Ruggeri *et al.*[16,17] The origin of this extra band is still unclear and we cannot exclude contamination, side chain absorbance or illumination effects. For sure, those discrepancies, shown in Fig. 6, are not solely due to the use of Au-tip. Thus, with the top-down configuration, there are band deformations and shifts mainly due to the illumination configuration and probably combined with the enhancement induced by the use of an Au-tip. Therefore, the top-down configuration should be

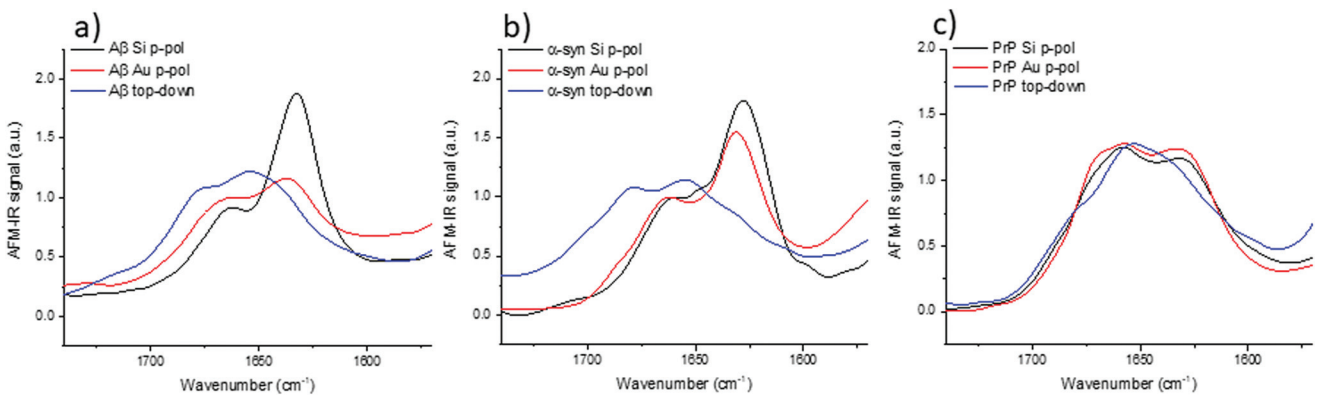

Fig. 6 Bottom-up illumination with an Si-tip (black curves) or an Au-tip (red curves) and top-down illumination with the Au-tip (blue curves), all data are obtained on p-pol: (a) Aβ, (b) α-syn and (c) PrP fibrils.

preferred for anisotropic sample or thick sample (<100 nm) due to its higher signal to noise but polarization effect should be considered for structural analysis. The bottom-up illumination should be preferred even with an Au-tip for highly-oriented proteins with thickness below 10 nm.

3.6 Structural analysis: comparison between ATR-FTIR and AFM-IR results

Previously, it has been demonstrated that structural analysis of amyloid fibrils could be performed using infrared spectroscopy like ATR-FTIR.[35]

In this section, the AFM-IR spectrum is compared with ATR-FTIR spectra. To evaluate the similarities between both spectra, hierarchical cluster analysis (HCA) is applied.[43] This method is commonly used to discriminate cell lines or gram type bacteria. The distance between each spectrum is calculated in the n-space domain, where n is the number of wavenumbers considered. An organigram is obtained with the distance between all spectra. Based on this organigram we can determine which AFM-IR setup provides the closest results to FTIR measurements looking at the position of the spectrum obtained for each setup compared with the ATR-FTIR one. In Fig. 7, the HCA results are presented for the different fibrils. For each fibril, the ATR-FTIR is in the center of the diagram in green and the closest spectra obtained with the different AFM-IR setups in blue. For the three proteins, the closest spectrum in the organigram is always the one obtained with the bottom-up configuration using a Si-tip and s-polarization while spectra obtained with the top-down illumination is always the farthest (in red Fig. 7). This quick analysis confirms that the bottom-up configuration using a Si-tip and s-pol is the most appropriated configuration to perform a structural analysis. Furthermore, in the case of PrP, the Euclidian distance between the different data are smaller than that for the other proteins (300 to 1000), confirming a smaller effect of the Au-tip or the top-down illumination for this sample.

To analyze the secondary structure of those samples, a curve fitting procedure was performed on both ATR-FTIR and AFM-IR spectra. The spectra are fitted with five components corresponding to the following secondary structures: β-sheet, random coil, α-helix, and two bands for the turns. The integral of each fitting bands provides the % of the different structures.

Fig. 8 shows the results for α-syn; the fitting procedure proposes that the β-sheet structure (maximum at 1628 cm^{-1}) represents: (i) 72% in the case of ATR-FTIR data and (ii) 73% in the case of AFM-IR data (bottom-up configuration with a Si-tip and s-pol). It is reported that this protein possess 73% of β-sheets.[25] In Table 2, the results of all spectra fitting of the different proteins are reported (the fitting and spectra are shown in Fig. SI 3–5†). First, the results obtained in the case of AFM-IR data (bottom-up configuration with a Si-tip and s-pol) are in good agreement with % of β-sheets calculated from the FTIR data. Second, this table clearly illustrates the high deviation that can be observed between bottom-up and top-down configurations. For example, only 17% β-sheet is identified for α-syn when fitting the data obtained in the top-down configuration.

The AFM-IR results with a Si-tip and a s-pol are always in good agreement with the ATR-FTIR, with only few % of errors, which is in the error of the method (around 10%).[11] The % of random and α-helix structures are given for information. As the exchange with deuterium was not done, it is difficult to differentiate those two structures from one another.[44]

3.7 Structural analysis of functional amyloid-like fibrils

The same investigations have been performed on a protein in bacteria called Hfq in which the C-terminal region is known to form amyloid-like fibrils.[45] This region is required for Hfq to form a membrane-associated coiled structure.[46] Unfortunately there is no high-resolution structure of this part of Hfq, only information based on infrared analysis of a solution that contains different aggregated species (from oligomers to fibrils). Unlike pathologic amyloid fibrils, Hfq amyloid structures appear only *in vitro* at a high concentration and the concentration of Hfq amyloid fibrils decreases with dilution. Therefore, there is an equilibrium between fibrillary species and other forms and a purification step of Hfq fibrils is required to perform structural analyses. This step is not required for AFM-IR experiments: thanks to the topography, fibrillar structures can be selected and the IR signature of this insoluble transitory structure can be obtained.

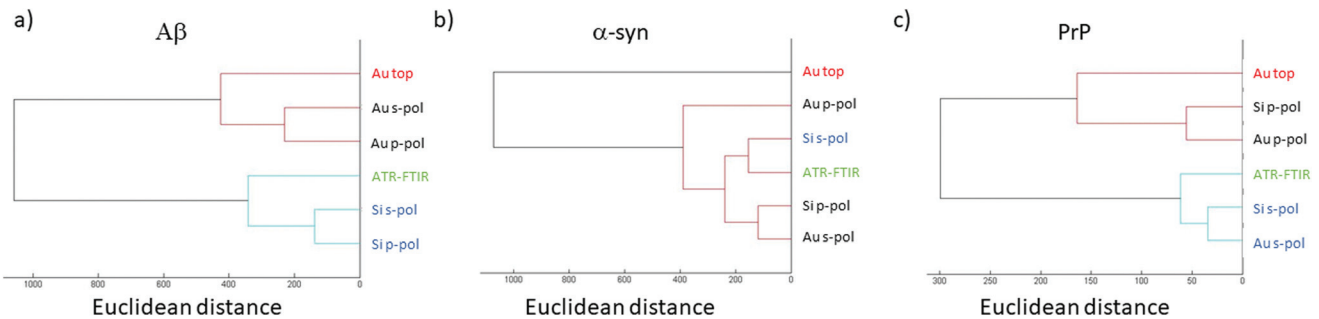

Fig. 7 Hierarchical cluster analysis for (a) Aβ, (b) α-syn and (c) PrP. The spectra are separated based on their Euclidean distance from each other (separation done on amide I band from 1700 to 1600 cm^{-1}). Shorter the connection is, the closer the spectra are. The name in green shows the ATR-FTIR spectra, in blue the closest spectra and in red the farthest.

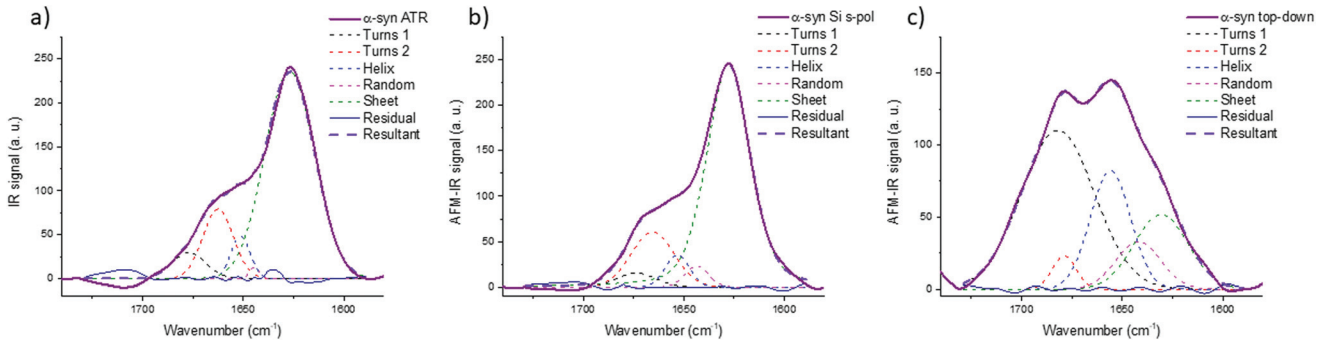

Fig. 8 Secondary structure analysis of α-syn: (a) ATR-FTIR, (b) AFM-IR bottom-up configuration with a Si-tip and s-pol and (c) AFM-IR with top-down illumination with Au-tip at p-pol. The colored dashed line corresponds to the curve fitting for the different components and solid line to the spectra, the results of the fitting are reported in Table 2.

Table 2 Curve fitting results for ATR-FTIR and AFM-IR spectra of the different amyloid fibrils. The β-sheet content in green is for the ATR-FTIR spectrum, in blue for the closest spectra and in red the farthest, as shown in Fig. 7. The corresponding curve fitting figures with all the fitting are available in the ESI Fig. SI 3–5 and Table SI 1†

α-Syn	ATR	Si s-pol	Top-down (p-pol)
Beta	72	73	17
Random	1	3	9
Alpha	6	5	21
Turns	21	19	53
Aβ	**ATR**	**Si s-pol**	**Top-down (p-pol)**
Beta	51	54	20
Random	30	22	15
Alpha	8	4	36
Turns	11	20	29
PrP	**ATR**	**Si s-pol**	**Top-down (p-pol)**
Beta	54	54	31
Random	0	8	13
Alpha	24	12	28
Turns	22	26	28

Fig. 9b shows the spectra obtained with a bottom-up configuration with a Si-tip and s-pol. The spectrum presents a maximum of absorption centered at 1612 cm^{-1} with two shoulders at 1637 and 1658 cm^{-1}. The spectra obtained with the four other AFM-IR configurations are presented in ESI Fig. SI 6.† The trend observed with Aβ is also observed in Hfq fibril spectra. That is, there is an important decrease of the ratio between the 1612 cm^{-1} band and the 1658 cm^{-1} band when using an Au-tip and a shift of frequency to higher wavenumber with the top-down illumination.

The structural analysis is thus performed using the spectra obtained with the bottom-up configuration with a Si-tip and s-pol. The results of the deconvolution are shown in Fig. 9b. The β-sheet content seems to be the major component and represents around 66% of the total structure. The rest of the assembly seems to have around 11% of random structure, 16% of α-helix and 7% of turns. The percentage of β-sheets from the ATR-FTIR is only 35%, 32% of random, 9% of α-helix and 24% of turns (Fig. 9a).

The percentage of β-sheet content obtained with ATR-FTIR is in good agreement with the one reported in the literature (42% in solution).[45] The difference observed may be explained as we worked on dried material in the present analysis. Nevertheless, the value obtained with AFM-IR is much higher (66%). This difference could come from the fact that the Hfq solutions are highly heterogeneous (easily observed during AFM measurements and already reported by Partouche *et al.*[19]) and the deposit contains several aggregated species. Here we

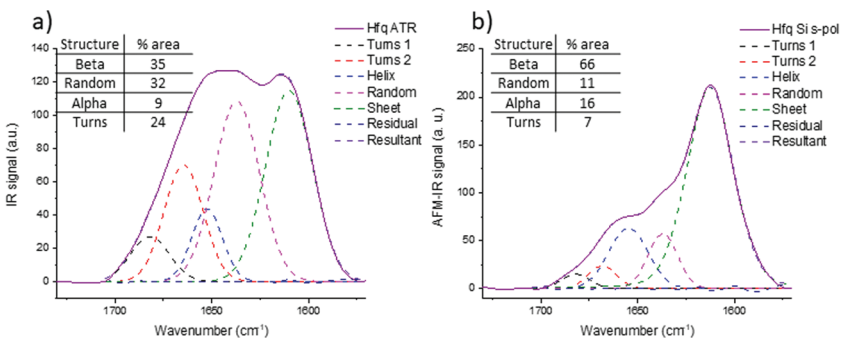

Fig. 9 Secondary structure analysis of Hfq: (a) ATR-FTIR, (b) AFM-IR bottom-up configuration with an Si-tip and s-pol. The dashed line corresponds to the curve fitting and the percentage of each structure are reported on the table on each spectrum.

clearly benefit from the high resolution offered by the system. AFM allows us to select directly the fibril shape, avoiding the aggregates, leading to a more accurate value for the β-sheet content of the fibrils.

4. Conclusion

For the first time, a complete study of three different amyloid fibrils (Aβ, α-syn and PrP) was performed using polarized resolved AFM-IR in different illumination configurations and using two types of AFM probes. Several other polarized-resolved AFM-IR studies,[41,47–55] were performed using either the bottom-up or top-down illumination configuration, but none of them has discussed in detail the effect of these different illumination and tip's gold-coating.

For the amyloid-like structure, only one team has presented results on a sample with a thickness of 150 nm (hundreds of fibrils), avoiding, at this scale, the gold enhancement effect.[52] The results presented here are related to nano-assemblies with a size below 10 nm which exhibit highly oriented chemical groups (here C═O bonds along the amyloid fibril axis).

The first parameter discussed is the influence of the incident polarization when using an Au-tip. We have seen that, due to the constraint of illumination, s-polarization leads to an orientation of the local electric field in the plane of the sample. While with a p-polarization the distribution of the local electric field is complex and possess two components, one vertical to the surface and a smaller one in the plane (due to P_z curvature and due to P_x contribution). For example, with Y-aligned amyloid fibril, the β-sheet structure is aligned along the *X*-axis and the stretching of the amide I is also Y-aligned, therefore at s-polarization the β-sheet absorption is detected but not at p-polarization although a fibril aligned on the *X*-axis can be detected by a p-polarization and not by the s-polarization.

Moreover, the model proposed shows that the gold-coating of the tip bends the electric field line in close proximity to the apex of the tip. It should only influence the sample at a short distance (3 nm). Thus, the global incident polarization is maintained for a thick sample (>100 nm) but it leads to a complex AFM-IR response for objects below 10 nm. Therefore, it is difficult to interpret the resulting spectra. For the moment, those models cannot explain the origin of the differences observed from one amyloid-like fibril to another as it does not take into account the orientation of the molecules themselves within the fibrils. If the model can be optimized in this direction, it might be able to explain the different results obtained on the Josephin domain of the ataxin-3 obtained with bottom-up illumination,[16] polyQ from huntingtin protein analyzed by top-down illumination,[17] Aβ42 fibrils obtained on bottom-up illumination[18] and Hfq obtained by top-down illumination.[19]

The second parameter discussed is the influence of the tip on the AFM-IR signal. In bottom-up illumination, either Si-tips or Au-tips (to locally enhance the electric field) could be used. We have shown that the signal obtained with the Au-tip is different from the one with the Si-tip. Unfortunately, this enhancement affects the local polarization and modifies the orientation of the electric field which leads to the deformation of the IR spectra for the oriented object. For example, with Aβ protein, $A_{1632/1662}$ decreases when the Au-tip is used. The orientation of the local enhanced electric fields induced by the gold does not match the orientation of the C═O vibration of the β-sheet structure. As a consequence, structural analysis of the spectrum obtained with the Au-tip seems difficult to trust and finally only spectra obtained with the Si-tip seems reliable.

The third point discussed is the illumination configuration. For the top-down illumination, only the Au-tip is used. As described previously, the gold coating has an influence on the IR spectra. The discrepancies observed with the Au-tip are more pronounced with the top-down illumination. Probably because of the excitation source feature, in bottom-up illumination, the excitation source is an evanescent wave whereas in top-down illumination the excitation is direct.

For the amyloid fibrils, the β-sheet band in the amide I region almost vanishes with top-down illumination. For fibrils with a high β-sheet content (Aβ, α-syn), the maximum of the amide I band shifts from 1630 cm^{-1} to 1655 cm^{-1} and a shoulder at 1720 cm^{-1} can be observed. For fibrils with a lower β-sheet content, the position of the amide I band seems to be conserved, but with a decrease of the β-sheet band around 1630 cm^{-1}. Due to the band deformation and the frequency shift with the top-down illumination and Au-tip, structural analysis seems compromised.

As a consequence, to structurally analyze amyloid fibrils, we suggest using a system with a bottom-up illumination, s-polarization and an Si-tip.

Indeed, the clustering analysis between the ATR-FTIR and AFM-IR spectra clearly demonstrate that the best similarities with the ATR-FTIR spectrum are obtained with the bottom-up illumination with the Si-tip and s-polarization, whereas the worst is obtained with the top-down configuration. To further quantify the similarities, structural analysis based on spectral deconvolution has been performed. The results clearly proved that the best solution to investigate the secondary structure of such protein assemblies is to use the AFM-IR set-up with a bottom-up illumination and Si-tips. In this case, the secondary structure analysis gives results comparable to ATR-FTIR with only a few percentages of difference. Furthermore, those results are even more robust if the polarization of the incident IR source is s-polarization especially for isolated fibrils. Based on this conclusion, we were able to analyze the structure of the Hfq fibrils with 10 nm diameter and length of few micrometers. Hfq only forms fibrils at a high concentration. Under this condition, the fibrils are probably not the major component of the mixture analyzed, and oligomers and non-amyloid Hfq forms are also present. By ATR-FTIR, only the averaged structures are probed, as we cannot differentiate species. With AFM-IR, the topography image allows us to select only the fibrils leading our analysis to estimate the

β-sheet content close to 64% clearly different from the 42% measured by ATR-FTIR.

Finally, in this paper, we have clearly demonstrated that gold-coated AFM probes are not recommended for fine structural analysis of isolated fibrils. Nevertheless, due to their better signal to noise ratio, the study of objects below 10 nm is easier with this configuration that remains perfectly relevant for non-oriented samples. Improving the signal to noise ratio without any change in the spectra is thus a major challenge. Different strategies have been already proposed, such as using a specifically designed tip with an internal resonator[56] or a new detection with a photonic transducer.[57] The better signal to noise ratio will improve the quality of the structural analysis and reduce the difference observed with ATR-FTIR. Indeed, the combination of the analysis of the morphology and infrared signature both at the nanoscale opens new possibility for characterization. The ability to analyze transitory or insoluble species based on their topographic selection is unique and AFM-IR is the most suited technique that will help with research on amyloidosis by providing deeper understanding of the secondary structure of proteins during aggregation kinetics.

Conflicts of interest

There are no conflicts to declare.

Acknowledgements

The authors thank FNRS "bourse de voyage" and De Brouckère-Solvay grant from ULB for financial support. The authors would like to thank R. R. Sinden for his help with the manuscript.

References

1 F. Chiti and C. M. Dobson, Protein Misfolding, Amyloid Formation, and Human Disease: A Summary of Progress Over the Last Decade, *Annu. Rev. Biochem.*, 2017, **86**(1), 27–68.
2 J. D. Sipe and A. S. Cohen, Review: History of the Amyloid Fibril, *J. Struct. Biol.*, 2000, **130**(2), 88–98.
3 L. Mucke, E. Masliah, G. Q. Yu, M. Mallory, E. M. Rockenstein, G. Tatsuno, K. Hu, D. Kholodenko, K. Johnson-Wood and L. McConlogue, High-level neuronal expression of abeta 1–42 in wild-type human amyloid protein precursor transgenic mice: synaptotoxicity without plaque formation, *J. Neurosci.*, 2000, **20**(11), 4050–4058.
4 J. D. Harper, S. S. Wong, C. M. Lieber and P. T. Lansbury, Observation of metastable Aβ amyloid protofibrils by atomic force microscopy, *Chem. Biol.*, 1997, **4**(2), 119–125.
5 F. L. Heppner, R. M. Ransohoff and B. Becher, Immune attack: the role of inflammation in Alzheimer disease, *Nat. Rev. Neurosci.*, 2015, **16**(6), 358–372.
6 A. Gustot, J. I. Gallea, R. Sarroukh, M. S. Celej, J.-M. Ruysschaert and V. Raussens, Amyloid fibrils are the molecular trigger of inflammation in Parkinson's disease, *Biochem. J.*, 2015, **471**(3), 323–333.
7 A. Gustot, V. Raussens, M. Dehousse, M. Dumoulin, C. E. Bryant, J.-M. Ruysschaert and C. Lonez, Activation of innate immunity by lysozyme fibrils is critically dependent on cross-β sheet structure, *Cell. Mol. Life Sci.*, 2013, **70**(16), 2999–3012.
8 E. Goormaghtigh, J. M. Ruysschaert and V. Raussens, Evaluation of the information content in infrared spectra for protein secondary structure determination, *Biophys. J.*, 2006, **90**(8), 2946–2957.
9 R. Sarroukh, E. Cerf, S. Derclaye, Y. F. Dufrene, E. Goormaghtigh, J. M. Ruysschaert and V. Raussens, Transformation of amyloid beta(1–40) oligomers into fibrils is characterized by a major change in secondary structure, *Cell. Mol. Life Sci.*, 2011, **68**(8), 1429–1438.
10 S. Krimm and J. Bandekar, Vibrational Spectroscopy and Conformation of Peptides, Polypeptides, and Proteins, in *Advances in Protein Chemistry*, ed. C. B. Anfinsen, J. T. Edsall and F. M. Richards, Academic Press, 1986, vol. 38, pp. 181–364.
11 A. Barth, Infrared spectroscopy of proteins, *Biochim. Biophys. Acta, Bioenerg.*, 2007, **1767**(9), 1073–1101.
12 E. Goormaghtigh, V. Cabiaux and J. M. Ruysschaert, Determination of soluble and membrane protein structure by Fourier transform infrared spectroscopy. III. Secondary structures, *Subcell. Biochem.*, 1994, **23**, 405–450.
13 J. J. Li and C. M. Yip, Super-resolved FT-IR spectroscopy: Strategies, challenges, and opportunities for membrane biophysics, *Biochim. Biophys. Acta, Biomembr.*, 2013, **1828**(10), 2272–2282.
14 A. Dazzi and C. B. Prater, AFM-IR: Technology and Applications in Nanoscale Infrared Spectroscopy and Chemical Imaging, *Chem. Rev.*, 2017, **117**(7), 5146–5173.
15 D. Galante, F. S. Ruggeri, G. Dietler, F. Pellistri, E. Gatta, A. Corsaro, T. Florio, A. Perico and C. D'Arrigo, A critical concentration of N-terminal pyroglutamylated amyloid beta drives the misfolding of Ab1–42 into more toxic aggregates, *Int. J. Biochem. Cell Biol.*, 2016, **79**, 261–270.
16 F. S. Ruggeri, G. Longo, S. Faggiano, E. Lipiec, A. Pastore and G. Dietler, Infrared nanospectroscopy characterization of oligomeric and fibrillar aggregates during amyloid formation, *Nat. Commun.*, 2015, **6**, 7831–7831.
17 F. S. Ruggeri, S. Vieweg, U. Cendrowska, G. Longo, A. Chiki, H. A. Lashuel and G. Dietler, Nanoscale studies link amyloid maturity with polyglutamine diseases onset, *Sci. Rep.*, 2016, **6**, 31155–31155.
18 S. Henry, N. B. Bercu, C. Bobo, C. Cullin, M. Molinari and S. Lecomte, Interaction of Aβ1–42 peptide or their variant with model membrane of different composition probed by infrared nanospectroscopy, *Nanoscale*, 2018, **10**(3), 936–940.
19 D. Partouche, J. Mathurin, A. Malabirade, S. Marco, C. Sandt, V. Arluison, A. Deniset-Besseau and S. Trepout,

Correlative infrared nanospectroscopy and transmission electron microscopy to investigate nanometric amyloid fibrils: prospects and challenges, *J. Microsc.*, 2019, **274**(1), 23–31.

20 J. Waeytens, V. Van Hemelryck, A. Deniset-Besseau, J.-M. Ruysschaert, A. Dazzi and V. Raussens, Characterization by Nano-Infrared Spectroscopy of Individual Aggregated Species of Amyloid Proteins, *Molecules*, 2020, **25**(12), 2899.

21 A. Dazzi, C. B. Prater, Q. Hu, D. B. Chase, J. F. Rabolt and C. Marcott, AFM–IR: Combining Atomic Force Microscopy and Infrared Spectroscopy for Nanoscale Chemical Characterization, *Appl. Spectrosc.*, 2012, **66**(12), 1365–1384.

22 F. Lu and M. A. Belkin, Infrared absorption nano-spectroscopy using sample photoexpansion induced by tunable quantum cascade lasers, *Opt. Express*, 2011, **19**(21), 19942–19947.

23 T. Lührs, C. Ritter, M. Adrian, D. Riek-Loher, B. Bohrmann, H. Döbeli, D. Schubert and R. Riek, 3D structure of Alzheimer's amyloid-β(1–42) fibrils, *Proc. Natl. Acad. Sci. U. S. A.*, 2005, **102**(48), 17342.

24 R. Sarroukh, E. Goormaghtigh, J. M. Ruysschaert and V. Raussens, ATR-FTIR: a "rejuvenated" tool to investigate amyloid proteins, *Biochim. Biophys. Acta*, 2013, **1828**(10), 2328–2338.

25 L. Bousset, L. Pieri, G. Ruiz-Arlandis, J. Gath, P. H. Jensen, B. Habenstein, K. Madiona, V. Olieric, A. Böckmann, B. H. Meier and R. Melki, Structural and functional characterization of two alpha-synuclein strains, *Nat. Commun.*, 2013, **4**, 2575.

26 H. Braak and E. Braak, Pathoanatomy of Parkinson's disease, *J. Neurol.*, 2000, **247**(Suppl 2), II3–I10.

27 M. Ingelsson, Alpha-Synuclein Oligomers—Neurotoxic Molecules in Parkinson's Disease and Other Lewy Body Disorders, *Front. Neurosci.*, 2016, **10**(408), DOI: 10.3389/fnins.2016.00408.

28 B. Caughey, G. S. Baron, B. Chesebro and M. Jeffrey, Getting a Grip on Prions: Oligomers, Amyloids, and Pathological Membrane Interactions, *Annu. Rev. Biochem.*, 2009, **78**(1), 177–204.

29 J. Collinge, Prion Diseases of Humans and Animals: Their Causes and Molecular Basis, *Annu. Rev. Neurosci.*, 2001, **24**(1), 519–550.

30 S. B. Prusiner, Prions, *Proc. Natl. Acad. Sci. U. S. A.*, 1998, **95**(23), 13363–13383.

31 G. Van der Rest, H. Rezaei and F. Halgand, Monitoring Conformational Landscape of Ovine Prion Protein Monomer Using Ion Mobility Coupled to Mass Spectrometry, *J. Am. Soc. Mass Spectrom.*, 2017, **28**(2), 303–314.

32 B. Lahiri, G. Holland and A. Centrone, Chemical Imaging Beyond the Diffraction Limit: Experimental Validation of the PTIR Technique, *Small*, 2013, **9**(3), 439–445.

33 J. C. Rodríguez-Pérez, I. W. Hamley and A. M. Squires, Infrared Linear Dichroism Spectroscopy on Amyloid Fibrils Aligned by Molecular Combing, *Biomacromolecules*, 2011, **12**(5), 1810–1821.

34 V. Sereda, M. R. Sawaya and I. K. Lednev, Structural Organization of Insulin Fibrils Based on Polarized Raman Spectroscopy: Evaluation of Existing Models, *J. Am. Chem. Soc.*, 2015, **137**(35), 11312–11320.

35 J. M. Ruysschaert and V. Raussens, ATR-FTIR Analysis of Amyloid Proteins, *Methods Mol. Biol.*, 2018, **1777**, 69–81.

36 J. Torrent, M. T. Alvarez-Martinez, M.-C. Harricane, F. Heitz, J.-P. Liautard, C. Balny and R. Lange, High Pressure Induces Scrapie-like Prion Protein Misfolding and Amyloid Fibril Formation, *Biochemistry*, 2004, **43**(22), 7162–7170.

37 O. V. Bocharova, L. Breydo, A. S. Parfenov, V. V. Salnikov and I. V. Baskakov, In vitro Conversion of Full-length Mammalian Prion Protein Produces Amyloid Form with Physical Properties of PrPSc, *J. Mol. Biol.*, 2005, **346**(2), 645–659.

38 E. A. Greenbaum, C. L. Graves, A. J. Mishizen-Eberz, M. A. Lupoli, D. R. Lynch, S. W. Englander, P. H. Axelsen and B. I. Giasson, The E46 K Mutation in α-Synuclein Increases Amyloid Fibril Formation, *J. Biol. Chem.*, 2005, **280**(9), 7800–7807.

39 M. S. Celej, R. Sarroukh, E. Goormaghtigh, G. D. Fidelio, J.-M. Ruysschaert and V. Raussens, Toxic prefibrillar α-synuclein amyloid oligomers adopt a distinctive antiparallel β-sheet structure, *Biochem. J.*, 2012, **443**(3), 719–726.

40 J. Torrent, D. Martin, S. Noinville, Y. Yin, M. Doumic, M. Moudjou, V. Béringue and H. Rezaei, Pressure Reveals Unique Conformational Features in Prion Protein Fibril Diversity, *Sci. Rep.*, 2019, **9**(1), 2802.

41 K. Hinrichs and T. Shaykhutdinov, Polarization-Dependent Atomic Force Microscopy-Infrared Spectroscopy (AFM-IR): Infrared Nanopolarimetric Analysis of Structure and Anisotropy of Thin Films and Surfaces, *Appl. Spectrosc.*, 2018, **72**(6), 817–832.

42 F. Lu, M. Jin and M. A. Belkin, Tip-enhanced infrared nanospectroscopy via molecular expansion force detection, *Nat. Photonics*, 2014, **8**, 307.

43 L. Mariey, J. P. Signolle, C. Amiel and J. Travert, Discrimination, classification, identification of microorganisms using FTIR spectroscopy and chemometrics, *Vib. Spectrosc.*, 2001, **26**(2), 151–159.

44 E. Goormaghtigh, V. Cabiaux and J.-M. Ruysschaert, Secondary structure and dosage of soluble and membrane proteins by attenuated total reflection Fourier-transform infrared spectroscopy on hydrated films, *Eur. J. Biochem.*, 1990, **193**(2), 409–420.

45 E. Fortas, F. Piccirilli, A. Malabirade, V. Militello, S. Trépout, S. Marco, A. Taghbalout and V. Arluison, New insight into the structure and function of Hfq C-terminus, *Biosci. Rep.*, 2015, **35**(2), e00190.

46 F. Wien, D. Martinez, E. Le Brun, C. N. Jones, S. Vrønning Hoffmann, J. Waeytens, M. Berbon, B. Habenstein and V. Arluison, The Bacterial Amyloid-Like Hfq Promotes In Vitro DNA Alignment, *Microorganisms*, 2019, **7**(12), 6639.

47 Z. Wang, B. Sun, X. Lu, C. Wang and Z. Su, Molecular Orientation in Individual Electrospun Nanofibers Studied

by Polarized AFM–IR, *Macromolecules*, 2019, **52**(24), 9639–9645.

48 E. Lipiec, A. Wnętrzak, A. Chachaj-Brekiesz, W. Kwiatek and P. Dynarowicz-Latka, High-resolution label-free studies of molecular distribution and orientation in ultrathin, multicomponent model membranes with infrared nano-spectroscopy AFM-IR, *J. Colloid Interface Sci.*, 2019, **542**, 347–354.

49 N. Piergies, E. Pięta, C. Paluszkiewicz, H. Domin and W. M. Kwiatek, Polarization effect in tip-enhanced infrared nanospectroscopy studies of the selective Y5 receptor antagonist Lu AA33810, *Nano Res.*, 2018, **11**(8), 4401–4411.

50 V. J. Rao, M. Matthiesen, K. P. Goetz, C. Huck, C. Yim, R. Siris, J. Han, S. Hahn, U. H. F. Bunz, A. Dreuw, G. S. Duesberg, A. Pucci and J. Zaumseil, AFM-IR and IR-SNOM for the Characterization of Small Molecule Organic Semiconductors, *J. Phys. Chem. C*, 2020, **124**(9), 5331–5344.

51 M. Roman, T. P. Wrobel, C. Paluszkiewicz and W. M. Kwiatek, Comparison between high definition FT-IR, Raman and AFM-IR for subcellular chemical imaging of cholesteryl esters in prostate cancer cells, *J. Biophotonics*, 2020, 13e201960094.

52 F. S. Ruggeri, C. Byrne, L. Khemtemourian, G. Ducouret, G. Dietler and Y. Jacquot, Concentration-dependent and surface-assisted self-assembly properties of a bioactive estrogen receptor α-derived peptide, *J. Pept. Sci.*, 2015, **21**(2), 95–104.

53 V. Giliberti, M. Badioli, A. Nucara, P. Calvani, E. Ritter, L. Puskar, E. F. Aziz, P. Hegemann, U. Schade, M. Ortolani and L. Baldassarre, Heterogeneity of the Transmembrane Protein Conformation in Purple Membranes Identified by Infrared Nanospectroscopy, *Small*, 2017, **13**(44), 1701181.

54 T. Shaykhutdinov, S. D. Pop, A. Furchner and K. Hinrichs, Supramolecular Orientation in Anisotropic Assemblies by Infrared Nanopolarimetry, *ACS Macro Lett.*, 2017, **6**(6), 598–602.

55 C.-T. Wang, B. Jiang, Y.-W. Zhou, T.-W. Jiang, J.-H. Liu, G.-D. Zhu and W.-B. Cai, Exploiting the Surface-Enhanced IR Absorption Effect in the Photothermally Induced Resonance AFM-IR Technique toward Nanoscale Chemical Analysis, *Anal. Chem.*, 2019, **91**(16), 10541–10548.

56 K. Kjoller, J. R. Felts, D. Cook, C. B. Prater and W. P. King, High-sensitivity nanometer-scale infrared spectroscopy using a contact mode microcantilever with an internal resonator paddle, *Nanotechnology*, 2010, **21**(18), 185705.

57 J. Chae, S. An, G. Ramer, V. Stavila, G. Holland, Y. Yoon, A. A. Talin, M. Allendorf, V. A. Aksyuk and A. Centrone, Nanophotonic Atomic Force Microscope Transducers Enable Chemical Composition and Thermal Conductivity Measurements at the Nanoscale, *Nano Lett.*, 2017, **17**(9), 5587–5594.

58 E. Hubin, S. Deroo, G. K. Schierle, C. Kaminski, L. Serpell, V. Subramaniam, N. van Nuland, K. Broersen, V. Raussens and R. Sarroukh, Two distinct beta-sheet structures in Italian-mutant amyloid-beta fibrils: a potential link to different clinical phenotypes, *Cell. Mol. Life Sci.*, 2015, **72**(24), 4899–4913.

59 A. Makky, L. Bousset, J. Polesel-Maris and R. Melki, Nanomechanical properties of distinct fibrillar polymorphs of the protein α-synuclein, *Sci. Rep.*, 2016, **6**, 37970–37970.

60 L. Breydo, N. Makarava and I. V. Baskakov, Methods for Conversion of Prion Protein into Amyloid Fibrils, in *Prion Protein Protocols*, ed. A. F. Hill, Humana Press, Totowa, NJ, 2008, pp. 105–115.

61 H. Rezaei, Y. Choiset, F. Eghiaian, E. Treguer, P. Mentre, P. Debey, J. Grosclaude and T. Haertle, Amyloidogenic Unfolding Intermediates Differentiate Sheep Prion Protein Variants, *J. Mol. Biol.*, 2002, **322**(4), 799–814.

